Computer Simulation Study of Two-Dimensional Polymer Solutions

Arun Yethiraj

Theoretical Chemistry Institute and Department of Chemistry, University of Wisconsin, Madison, Wisconsin 53706

Received December 3, 2002; Revised Manuscript Received May 28, 2003

ABSTRACT: Monte Carlo simulations are reported for the conformational properties, static structure, and equation of state of two-dimensional polymers. The polymer molecules are modeled as chains of freely jointed tangent hard disks. For isolated chains, the scaling of the mean-square radius of gyration, R_g^2, with degree of polymerization, n, is consistent with $R_g^2 \sim n^{3/2}$. Over the range of concentrations and chain lengths studied, the chains do not behave as ideal chains, with $R_g^2 \sim n^{1.07\pm0.03}$ at the highest concentration studied. Surprisingly, for very high concentrations, the chain size increases with increasing concentration. Contrary to expectations, the chains do not become disklike at high concentrations, and the asphericity changes by only about 10% over the entire range of concentrations. In fact, the distribution of shapes of the chains remains essentially unchanged as the concentration is increased, and there is considerable interpenetration between polymer molecules. Results are also presented for the pair correlation functions and the equation of state. The osmotic pressure, p, scales with concentration, c, as $p \sim c^{4.7\pm0.1}$, which is stronger than the scaling prediction of $p \sim c^3$.

I. Introduction

The behavior of confined polymers is a subject of considerable current interest.[1] A special case is when the polymers are sufficiently constrained that they are almost two-dimensional. Such a situation is realized, for example, when DNA molecules are adsorbed to the surface of charged lipid bilayers. A series of recent experiments[2−4] have studied the conformational properties of DNA molecules on lipid bilayers using fluorescence microscopy. The scaling of the chain size with degree of polymerization and the behavior of the single chain structure factor demonstrate that these chains are two-dimensional in nature. The experiments provide detailed information about chain conformations in dilute solutions but are unable to resolve intermolecular packing and structure in semidilute solutions. In this article, we present a computer simulation study of the chain conformations, static structure, and volumetric properties of an off-lattice model of two-dimensional polymers.

The size of polymer chains displays characteristic behavior in different concentration regimes. In dilute solutions, the chains are essentially isolated, and the chain size, characterized by the root-mean-square radius of gyration, R_g, scales with degree of polymerization, n, as $R_g \sim n^{\nu_F}$, where $\nu_F = 0.588$ and 0.75 for $d = 3$ and 2, respectively, where d is the dimensionality of space. As the concentration is increased, individual chains begin to overlap. In the semidilute regime, for $d = 3$, chains interpenetrate and the properties are dominated by the correlation length, ξ, which is independent of n. In this regime the chains are also ideal, i.e., $R_g^2 \sim n$.

Two scenarios for chain conformations in two dimensions have been suggested. In the first, it is argued that chains cannot interpenetrate for $d = 2$, and therefore polymer molecules must be segregated disks.[5] In this model, in nondilute solutions, the chains contract while still in contact with each other as the concentration is increased. Since the fraction of area per chain is constant, this implies that $R_g^2 \sim c^{-1}$ and $R_g^2 \sim n$. This segregation also results in a very deep correlation hole because other chains are essentially excluded from a region of the order of the size of a single chain. Scaling theory, on the other hand, relies on interpenetration of molecules in the semidilute regime.[6] The overlap threshold concentration, c^*, is given by $c^* \approx n/R_g^2 \sim n^{-1/2}$. For $c > c^*$ $R_g^2 \sim n^{3/2}(c/c^*)^m$, where m is chosen so that the chains are ideal, i.e., $R_g^2 \sim n$. This gives $m = -1$ and therefore $R_g^2 \sim c^{-1}$. Logarithmic corrections to scaling are predicted in two-dimensional systems.[7] Interestingly, the scaling relations for chain size, i.e., $R_g^2 \sim c^{-1}$ and $R_g^2 \sim n$, are the same in both the pictures, and so the variation of chain size with concentration and degree of polymerization cannot be used to distinguish between these models.

One can develop a scaling theory for the osmotic pressure, p, as a function of concentration.[6] In dilute solutions the ideal gas law gives $p = c/n$. In the semidilute regime we expect that the pressure will be independent of the degree of polymerization. Starting with the ansatz $p \sim (c/n)(c/c^*)^m$, m is chosen so that $p \sim n^0$ in the semidilute regime. This gives $m = 2$ and therefore $p \sim c^3$. The dependence of pressure on concentration is predicted to be much stronger than the three-dimensional case where $p \sim c^{9/4}$.

There have been a few lattice simulations of lattice models of two-dimensional polymer solutions.[8−15] Dickman[8,9] performed simulations of two-dimensional chains between surfaces in order to study the equation of state. Carmesin and Kremer[10] performed bond fluctuation lattice model simulations of two-dimensional polymers and concluded that the chains were segregated and each molecule homogeneously filled a fluctuating disklike region, consistent with the de Gennes prediction.[5] At high concentrations, however, they found that $R_g^2 \sim n$ and that the single chain structure factor $\hat{\omega}(k) \sim k^{-2}$, which taken together are consistent with ideal chain behavior rather than the behavior of disklike objects. For melts $R_g^2 \sim n^{2\nu}$ with $\nu \approx 0.5$ is observed in other simulations as well, although the actual values range from $\nu = 0.52$ to 0.55.[11−13] Teraoka and Wang[13] studied the concentration dependence of chain size for various chain lengths and found significant deviations from

10.1021/ma025907r CCC: $25.00
Published on Web 07/02/2003

scaling predictions for finite concentrations. These deviations from scaling could be due to the logarithmic corrections predicted by Nikamarov and Obukhov.[7] More recent simulations find that the chains are *not* segregated at meltlike concentrations but interpenetrate significantly. There are therefore significant differences between the various simulations for this system. The experiments on semidilute solutions[3] do not shed light on these issues because they do not report detailed analyses of chain conformations. There have been two off-lattice simulations of two-dimensional polymers,[16,17] where only short chains ($n = 5$ and 20) were studied. Equations of state for off-lattice two-dimensional polymers have been developed[18,19] that are in good agreement with the off-lattice simulation results.

In this paper, we present extensive computer simulation results for an off-lattice model of two-dimensional polymers. The molecules are modeled as freely jointed chains of tangent hard disks of diameter σ, and the static properties are obtained from Monte Carlo simulations. We employ a one-component model for the polymer solution, i.e., the solvent is treated as a continuum, and is a very *good* solvent for the polymers (the χ parameter is equal to zero). The concentration, c, defined as $c = nN/A$ where N is the number of chains and A is the area, is therefore also the site density of the fluid, and the osmotic pressure, p, is also the system pressure. Chains lengths, n, ranging from $n = 16$ to 256, and area fractions, ϕ (defined as $\phi \equiv \pi\sigma^2 c/4$), ranging from $\phi = 0$ to 0.65, are investigated.

Some of the simulation results are as expected, and some are surprising. For short chains there is no semidilute regime; i.e., the internal chain concentration is always higher than the overall chain concentration. For longer chains $R_g^2 \sim n^{1.07\pm0.03}$ in the semidilute regime, consistent with previous simulations, although an analysis of the single chain structure factor shows that the chains are not ideal at these concentrations. At all concentrations a variety of configurations, ranging from disklike to extended, are found. In fact, the chain shape and distribution of shapes are relatively insensitive to concentration. Interestingly, at very high concentrations, the chain size is an increasing function of concentration. In the simulations, $p \sim c^{4.7\pm0.1}$ in the semidilute regime; scaling theory is not consistent with this result.

The rest of this paper is organized as follows. The Monte Carlo simulations are described in section II, simulation results are presented in section III, and some conclusions are presented in section IV.

II. Monte Carlo Simulations

The simulation cell is a square with area L^2 with periodic boundary conditions in both x and y directions. The polymer molecules are modeled as freely jointed tangent-hard-disk chains with bond length and disk diameter of σ. We choose our length scale by setting $\sigma = 1$. The systems consists of N chains of length n. Simulations are performed for n ranging from 16 to 256 and with either 20 or 50 chain molecules.

Initial configurations are generated by a growth and equilibration algorithm.[20] N disks of diameter σ are first inserted into the simulation cell, and attempts are made to grow them into chains. This method works well for low area fractions and short chains but fails for long chains at high area fractions when the growing of chains becomes difficult. Initial configurations for these state points are created by starting with a low-density configuration and compressing them via simulations in the isobaric−isothermal ensemble.

Simulations are performed in the canonical (NAT fixed where T is the temperature) and isobaric−isothermal (NpT fixed) ensembles. The canonical ensemble simulations are a standard application of the Metropolis algorithm and similar to that used in previous work on three-dimensional polymer melts.[21] A molecule is chosen at random, and an attempt is made to move it using either a Dickman−Hall,[22] continuum configurational bias,[23] or reptation move,[24] adapted to two-dimensional systems. The move is accepted if there is no overlap between the sites of the trial chain and existing chains. The additional feature in the NpT simulations is that area change moves are performed, and this is done according to the algorithm described by Frenkel and Smit.[25] A chain move or area change move is chosen randomly with a 1% probability (on average) of the latter. In the area change moves the two linear dimensions of the cell are scaled by the same amount, and the chain centers of mass are placed so that their positions (relative to the box) are the same as before. The chain conformations are not changed, but the move can result in intermolecular overlap between the chains. If the move does not result in an overlap, it is accepted with probability $e^{-\beta H}$, where $H = p(A_n - A_0) - (N + 1)\ln(A_n/A_0)$; A_0 is the area of the system before the move, and A_n is the area with the attempted area change.

Each simulation proceeds as follows. First, an initial configuration is generated and equilibrated. It is considered to be equilibrated if the average size and pressure (in NAT simulations) or density (in NpT simulations) reach a steady value. The mean-square displacement of the chain centers of mass is monitored and the center-of-mass diffusion constant calculated. Properties are then averaged over runs and performed in sets of 1 million attempted moves, long enough so that on average the chains have moved at least one radius of gyration. The length of the runs depends strongly on the state point and chain length. For $n = 16$ and area fraction $\phi = 0.1$ only 2−3 million attempted moves are required, but for $n = 256$ and $\phi = 0.3$, 500 million attempted moves are required. The upper limit of area fractions studied is restricted by the ability of the algorithm to evolve the system in a reasonable time.

Several tests are performed to check the validity of the results. In the NpT simulations, the pressure is fixed and the area fluctuates. The pressure is also calculated from the correlation functions using the virial theorem (described below). We make sure that the virial pressure is identical to the set pressure within statistical uncertainty, usually to two decimal places. For some state points, simulations are performed for both system sizes, i.e., $N = 20$ and 50, to check for finite size effects, which are found to be negligible and well within statistical uncertainty.

Several properties are monitored in the simulations. The mean-square end-to-end distance, $\langle R^2 \rangle$, and mean-square radius of gyration are calculated from

$$\langle R^2 \rangle = \frac{1}{N}\sum_{i=1}^{N}\langle(\mathbf{r}_n^i - \mathbf{r}_1^i)^2\rangle \qquad (1)$$

$$R_g^2 = \frac{1}{Nn}\sum_{i=1}^{N}\sum_{j=1}^{n}\langle(\mathbf{r}_j^i - \mathbf{r}_{cm}^i)^2\rangle \quad (2)$$

where $\mathbf{r}_j^i$ is the position of bead j on chain i, $\mathbf{r}_{cm}^i$ is the position of the center-of-mass of chain i, and $\langle\mathcal{A}\rangle$ denotes an ensemble average of the quantity $\mathcal{A}$.

The shape of the chains is characterized by the asphericity.[26] For each chain, i, the elements of the radius of gyration tensor, $\mathbf{T}$, are given by

$$T_{kl} = \frac{1}{n}\sum_{j=1}^{n}(\mathbf{r}_{j,k}^i - \mathbf{r}_{cm,k}^i)\cdot(\mathbf{r}_{j,l}^i - \mathbf{r}_{cm,l}^i) \quad (3)$$

where k and l are the coordinates x and y, $\mathbf{r}_{j,k}^i$ is the kth coordinate of the position $\mathbf{r}_j^i$, and $\mathbf{r}_{cm,k}^i$ is the kth coordinate of the center-of-mass of chain i. The tensor $\mathbf{T}$ has two eigenvalues, which are denoted λ_1 and λ_2 with the convention $\lambda_1 \geq \lambda_2$. The asphericity, A_2, is given by

$$A_2 = \frac{\langle(\lambda_2 - \lambda_1)^2\rangle}{\langle(\lambda_2 + \lambda_1)^2\rangle} \quad (4)$$

where the average here is over the ensemble *and* over all chains. The normalization ensures that $A_2 = 1$ for a rod (line) and $A_2 = 0$ for a disk. We also monitor the probability distribution function for these eigenvalues, denoted $P_1(\lambda)$ and $P_2(\lambda)$, for the larger and smaller eigenvalues, respectively.

The average site−site pair correlation function, $g(r)$, is obtained from

$$g(r) = \frac{1}{c^2}\sum_{\alpha=1}^{n}\sum_{\gamma=1}^{n}\sum_{i=1}^{N}\sum_{j\neq i}\langle\delta(\mathbf{r}_\alpha^i)\,\delta(\mathbf{r}_\gamma^j - \mathbf{r})\rangle \quad (5)$$

where c is the number of sites per unit area and $\delta(\mathbf{r})$ is the Dirac delta function. The nonbonded contribution to the average intramolecular correlation function, denoted $\omega_{nb}(r)$, is calculated from

$$\omega_{nb}(r) = \frac{1}{Nn}\sum_{i=1}^{N}\sum_{|k-j|>1}\langle\delta(\mathbf{r}_j^i - \mathbf{r}_k^i - \mathbf{r})\rangle \quad (6)$$

and the single chain static structure factor is obtained from the discrete Fourier transform:

$$\hat{\omega}(k) = 1 + 2\left(1 - \frac{1}{n}\right)J_0(k\sigma) + 2\pi\Delta\sum_i r_i\omega_{nb}(r_i)J_0(kr_i) \quad (7)$$

where $J_0(x)$ is the Bessel function of zeroth order, Δ is the bin size of the histogram that contains $\omega_{nb}(r)$, and $r_i = (2i - 1)\Delta/2$.

In the NAT simulations, the pressure is obtained from the virial theorem.[27,28] By a straightforward extension of the scaling method to two-dimension systems, it can be shown that the pressure is given by

$$\beta p = \rho - \frac{\pi}{2}\rho^2\int_0^\infty r^2\frac{d\beta v(r)}{dr}f(r) \quad (8)$$

where $\beta = 1/k_BT$, k_B is Boltzmann's constant, $v(r)$ is the interaction potential, and $\rho = N/A$ is the chain number density. The function $f(r)$ is given by

$$f(r) = \frac{1}{c^2}\sum_{\alpha=1}^{n}\sum_{\gamma=1}^{n}\sum_{i=1}^{N}\sum_{j\neq i}\langle\delta(\mathbf{r}_\alpha^i)\,\delta(\mathbf{r}_\gamma^j - \mathbf{r})(\mathbf{r}_{11}^{ij}\cdot\hat{\mathbf{r}})\rangle \quad (9)$$

where $\mathbf{r}_{11}^{ij} = \mathbf{r}_1^i - \mathbf{r}_1^j$ and $\hat{\mathbf{r}} = \mathbf{r}/|\mathbf{r}|$. For the special case of two-dimensional hard-disk chains, the compressibility factor, $\beta p/\rho$, is given by

$$\frac{\beta p}{\rho} = 1 + 2n\phi f(\sigma^+) \quad (10)$$

The function $f(r)$ is monitored in the simulations and $(r - \sigma)^m f(r)$ (where m is a constant) is extrapolated to contact. For each case, the constant m is adjusted between $m = 1$ and $m = 4$ so that the extrapolated function is roughly linear near $r = \sigma$.

The simulation results for the average chain size, asphericity, and pressure are summarized in Tables 1, 2, and 3. Lengths are measured in units of σ, and the reduced pressure, p^*, is defined as $p^* = \beta p\sigma^3$. Statistical uncertainties are obtained from block averages and are reported as one standard deviation in the tables and two standard deviations in the figures. In some cases the value of pressure is not listed, and this is because the pair correlations are not monitored in those (canonical ensemble) simulations. This is because calculating the pair correlation, which scales as the square of the number of sites whereas the simulation itself scales linearly in the number of sites, is computationally intensive. Zero-density results are obtained from simulations of a single isolated chain using the same algorithm as that used for the many-chain system.

Table 1. Summary of Simulation Results for Chain Conformations and Volumetric Properties for $n = 16$

ϕ	$\langle R^2\rangle$	R_g^2	A_2	p^*
0.00	61.43 ± 0.36	8.30 ± 0.03	0.64 ± 0.01	0
0.10	59.30 ± 0.53	8.13 ± 0.04	0.64 ± 0.01	0.013 ± 0.001
0.20	55.09 ± 0.63	7.78 ± 0.05	0.62 ± 0.01	0.049 ± 0.005
0.30	50.41 ± 0.76	7.35 ± 0.06	0.61 ± 0.01	0.144 ± 0.003
0.40	44.80 ± 0.75	6.82 ± 0.08	0.59 ± 0.01	0.36 ± 0.02
0.50	39.40 ± 1.87	6.24 ± 0.15	0.58 ± 0.02	0.88 ± 0.04
0.60	34.30 ± 3.16	5.65 ± 0.26	0.57 ± 0.03	2.14 ± 0.04
0.65	32.32 ± 3.61	5.39 ± 0.31	0.57 ± 0.04	

Table 2. Summary of Simulation Results for Chain Conformations and Volumetric Properties for $n = 32$

ϕ	$\langle R^2\rangle$	R_g^2	A_2	p^*
0.00	180.69 ± 1.21	24.44 ± 0.08	0.63 ± 0.01	0
0.05	175.26 ± 2.01	24.05 ± 0.17	0.63 ± 0.01	0.0027 ± 0.0003
0.10	167.65 ± 1.81	23.37 ± 0.13	0.62 ± 0.01	0.008 ± 0.0009
0.15	158.87 ± 2.09	22.54 ± 0.16	0.62 ± 0.01	0.019 ± 0.002
0.20	146.82 ± 2.93	21.48 ± 0.23	0.60 ± 0.01	0.036 ± 0.003
0.25	135.74 ± 3.49	20.37 ± 0.27	0.59 ± 0.01	0.067 ± 0.005
0.30	124.63 ± 4.59	19.16 ± 0.41	0.59 ± 0.02	0.116 ± 0.003
0.35	113.56 ± 4.97	18.07 ± 0.42	0.58 ± 0.02	0.20 ± 0.01
0.40	103.11 ± 6.80	16.78 ± 0.56	0.57 ± 0.02	0.32 ± 0.01
0.45	93.25 ± 7.01	15.61 ± 0.68	0.56 ± 0.03	0.52 ± 0.02
0.50	87.04 ± 9.46	14.81 ± 0.79	0.56 ± 0.04	0.82 ± 0.03
0.55	80.81 ± 8.85	13.93 ± 0.94	0.56 ± 0.05	1.23 ± 0.04
0.60	71.80 ± 5.67	12.92 ± 0.50	0.57 ± 0.03	2.08 ± 0.07
0.625	76.59 ± 6.16	13.20 ± 0.51	0.58 ± 0.04	
0.65	78.72 ± 6.27	13.79 ± 0.24	0.60 ± 0.02	3.36 ± 0.12

III. Results and Discussion

A. Chain Dimensions. For isolated chains $R_g^2 \sim n^{2\nu}$, with $\nu = 3/4$, and as the area fraction is increased, the exponent ν decreases. Figure 1 is a log−log plot of R_g^2 as a function of $n - 1$ for various values of ϕ. The lines

Table 3. Summary of Simulation Results for Chain Conformations and Volumetric Properties for $n = 64$, 128, and 256

n	ϕ	$\langle R^2 \rangle$	R_g^2	A_2	p^*
64	0	518 ± 3	70.8 ± 0.2	0.634 ± 0.003	0
64	0.1	458 ± 17	65.4 ± 1.6	0.61 ± 0.02	0.0052 ± 0.0009
64	0.2	357 ± 18	56.2 ± 1.7	0.58 ± 0.02	0.029 ± 0.003
64	0.3	260 ± 8	44.4 ± 0.9	0.55 ± 0.03	0.106 ± 0.005
64	0.453 ± 0.005	201 ± 37	35.5 ± 3.2	0.53 ± 0.08	0.5
64	0.497 ± 0.006	176 ± 26	32.4 ± 2.7	0.53 ± 0.08	0.77
64	0.525 ± 0.005	166 ± 26	30.5 ± 2.6	0.51 ± 0.06	1.00
64	0.568 ± 0.005	178 ± 29	30.6 ± 2.6	0.56 ± 0.07	1.50
64	0.599 ± 0.004	170 ± 30	31.4 ± 1.3	0.62 ± 0.04	2.00
128	0	1476 ± 30	204 ± 3	0.634 ± 0.009	0
128	0.1	1175 ± 68	174 ± 6	0.6 ± 0.03	0.0035 ± 0.0009
128	0.2	819 ± 103	136 ± 9	0.57 ± 0.05	0.024 ± 0.005
128	0.3	614 ± 19	105 ± 4	0.57 ± 0.04	0.096 ± 0.003
128	0.364 ± 0.004	504 ± 74	88 ± 7	0.54 ± 0.06	0.2
128	0.454 ± 0.004	419 ± 47	77 ± 6	0.55 ± 0.06	0.5
256	0	4160 ± 397	577 ± 54	0.62 ± 0.05	0
256	0.1	2989 ± 510	465 ± 54	0.60 ± 0.08	
256	0.2	1581 ± 250	288 ± 25	0.53 ± 0.08	
256	0.3	1170 ± 216	224 ± 17	0.55 ± 0.07	
256	0.366 ± 0.004	974 ± 88	184 ± 5	0.54 ± 0.03	0.2
256	0.454 ± 0.001	632 ± 30	152 ± 1	0.523 ± 0.008	0.5

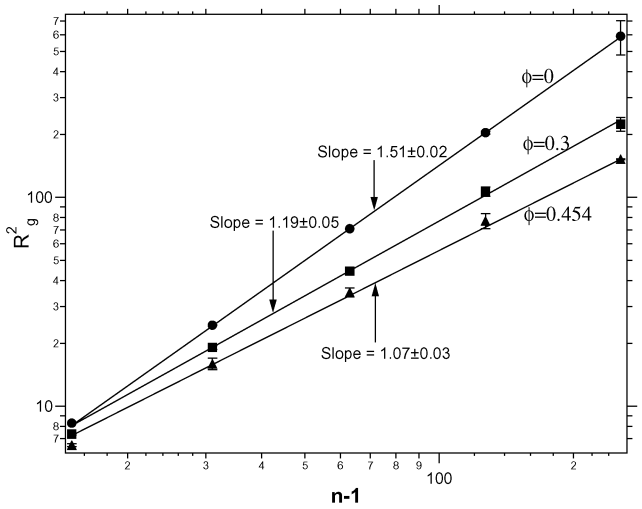

Figure 1. Variation of the mean-square radius of gyration with chain length for various area fractions, ϕ. The lines are least-squares fits to the data for $n \geq 64$ with slopes (as marked).

are least-squares linear fits for $n \geq 64$. For $\phi = 0$, the self-avoiding walk exponent is observed, within statistical uncertainties, for the chain lengths considered, suggesting that the simulations are probably in the scaling regime of long chains. As the area fraction is increased, the exponent decreases to 1.19 ± 0.05 and 1.07 ± 0.03 for $\phi = 0.3$ and 0.454; such a trend is expected from theory. We do not observe ideal scaling even at the highest area fraction studied, consistent with previous simulation studies.[10−12] It cannot be ruled out, of course, that ideal scaling might achieved for higher values of the area fraction or for longer chains.

A important issue is the value of the overlap threshold area fraction, ϕ^*, in these systems. Following des Cloizeaux and Jannink,[6] one can define the overlap threshold monomer concentration as the concentration for which the internal concentration $c^* = 2n/\langle R^2 \rangle$ becomes equal to the overall concentration. In terms of area fractions, this is when $\phi^* = \pi n/2\langle R^2 \rangle$. With this definition, ϕ^* can be estimated from the data in Tables 1−3, and we find that the internal area fraction is greater than the overall area fraction over the entire range of area fractions studied; i.e., the solutions are always "dilute" in the sense that $\phi < \phi^*$ for all the chain lengths studied! If one uses the alternative definition[6] $\phi^* = \pi n/12R_g^2$, then for $n < 128$, $\phi < \phi^*$ over the entire range of concentrations studied, and $\phi^* \approx 0.44$ and 0.37 for $n = 128$ and 256, respectively. Finally, if we assume that a single chain occupies a disk of radius $R = R_g$, then $\phi^* \approx n\sigma^2/4R_g^2$, $\phi < \phi^*$ for $n = 16$ and 32, and $\phi^* \approx$ 0.45, 0.3, and 0.25 for $n = 64$, 128, and 256, respectively.

Teraoka and Wang (TW) use a definition of the overlap threshold concentration that is based solely only on the size of the chains at infinite dilution. For the molecular model of this work, the TW definition is

$$\phi^\dagger = \frac{\pi n}{8\left(R_{g0} + \frac{R_{g0}}{2R_0}\right)^2} \tag{11}$$

where R_{g0} and R_0 are respectively the root-mean-square radius of gyration and root-mean-square end-to-end distance at infinite dilution, and $R_{g0}/2R_0 \approx 0.1838$ for freely jointed hard disk chains. We use a different symbol for the TW overlap threshold concentration, i.e., $\phi^\dagger$ instead of ϕ^*, because this is not how the overlap threshold concentration is usually defined. Note that by construction $\phi^\dagger \sim n^{-1/2}$, in accord with scaling theory. We employ this definition of the overlap threshold concentration because it allows us to scale the data for all chain lengths. We find that $\phi^\dagger = 0.67$, 0.48, 0.34, 0.24, and 0.17 for $n = 16$, 32, 64, 128, and 256, respectively.

Figure 2 is a log−log plot of R_g^2/R_{g0}^2 with $\phi/\phi^\dagger$ for various chain lengths. According to scaling theory, $R_g^2 \sim \phi^{-1}$ in two-dimensional systems while $R_g^2 \sim \eta^{-1/4}$ in three dimensions (η is the volume fraction). The sharper drop in size in two-dimensional systems can be qualitatively explained by noting that interpenetration is more difficult in two dimensions, and this results in a greater tendency for the chains to fold into themselves. The line in Figure 2 is a least-squares fit to the data for $\phi/\phi^\dagger \geq 1.25$. Although the fit weights the data for short chains more heavily (because the statistical uncertainties are smaller) a good fit is obtained, and the slope of the line is −1.0 ± 0.1.

An interesting feature is that at very high area fractions the chain size *increases* as the area fraction is increased. This is seen in the inset of Figure 2, which depicts R_g^2 as a function of ϕ for $n = 32$. Such behavior

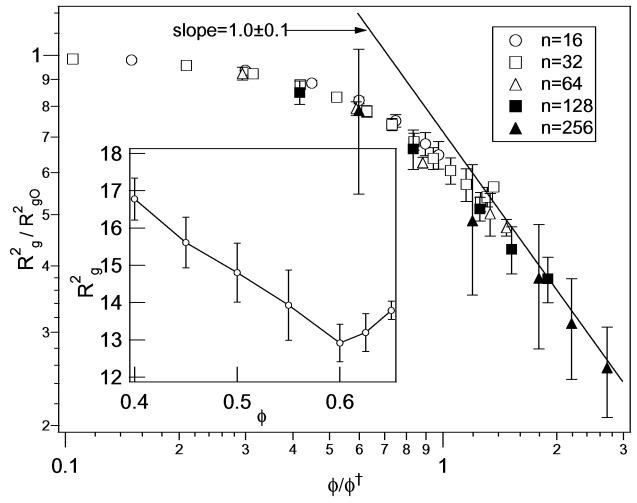

Figure 2. Scaling plot for the variation of chain size with area fraction. The mean-square radius of gyration divided by the value for $\phi = 0$ is plotted against the area fraction divided by a quantity related to the overlap threshold area fraction (see text for definition). The line is a least-squares fit to the data for $\phi/\phi^\dagger > 1.25$ with slope as marked. The inset shows R_g^2 for $n = 32$. Error bars are two standard deviations about the mean.

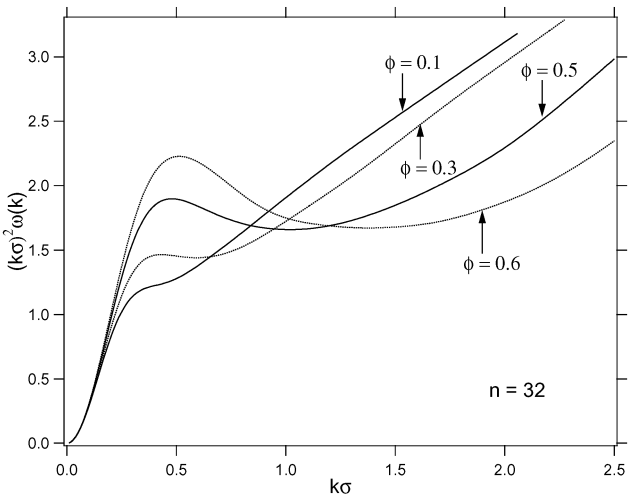

Figure 3. Kratky plot of the single chain structure factor for $n = 32$ and various area fractions (as marked).

is predicted by integral equation theories for three-dimensional polymer melts[29] but has never, to our knowledge, been observed in simulations or in experiments. The reason for this behavior (in the theory) is as follows. In the integral equation theory, the many-chain system is replaced by a single chain that interacts via a (self-consistently determined) pairwise decomposable "solvation" potential that (approximately) accounts for the effect of the other chains. At low and intermediate concentrations, the solvation potential is purely attractive, and this results in a decrease in the chain size. As the concentration is increased, the solvation potential displays oscillatory spatial variation as a consequence of the packing of the chains on a monomeric length scale. At very high concentrations, the second minimum in the solvation potential is sufficiently deep that some more extended conformations become favored. This results in an expansion of chains at very high densities. For freely jointed hard chains, the theory predicts that the chain size will increase with increasing density for volume fractions greater than about 0.55, and such high concentrations are impossible to attain in computer simulations for $d = 3$. Such high concentrations are accessible in $d = 2$, and it is possible that a similar physical reason is responsible for the high-density behavior seen in Figure 2.

B. Single Chain Structure Factor. Single chain conformational properties are often analyzed in terms of the single chain structure factor, $\hat{\omega}(k)$. Consider a disk of radius r around a central bead so that m beads are present inside the disk. If $r^2 \sim m^{2\nu}$, then $\omega(r) \sim m/r^d$ implies $\omega(r) \sim r^{1/\nu - d}$. Taking the Fourier transform and using the scaling trick, one obtains $\hat{\omega}(k) \sim k^{-1/\nu}$ over the range of length scales of the order of the size of the chain. For an ideal chain, $\nu = {}^1/_2$ and $k^2\hat{\omega}(k) \sim 1$ in the scaling regime. It is therefore customary to plot $k^2\hat{\omega}(k)$ vs k on what is called a Kratky plot.

Figure 3 is a Kratky plot for $n = 32$ and $\phi = 0.1$, 0.3, 0.5, and 0.6. For low wave vectors, $kR_g \ll 1$, it is expected[30] that $k^2\hat{\omega}(k) \sim nk^2(1 - k^2R_g^2/3 + ...)$, and in Figure 3 the low-k behavior is similar for all values of ϕ. For large wave vectors $\hat{\omega}(k) \sim 1$ in all cases. The interesting regime is the intermediate (scaling) regime. In all the curves in Figure 3, $k^2\hat{\omega}(k)$ rises to a maximum or plateau for $kR_g \sim 1$. As ϕ increases, this peak or plateau occurs at a larger value of k and has a larger amplitude, which is because the chains are more compact for larger values of ϕ (note that in the plateau regime $k^2\hat{\omega}(k) \sim 2n/R_g^2$ for an ideal chain). For $\phi = 0.1$ there is hardly any plateau, and $k^2\hat{\omega}(k)$ is an increasing function of k in the scaling regime, consistent with a value of $\nu > 0.5$. As the area fraction is increased, for $\phi = 0.3$, the curve shows a distinct plateau regime and looks very similar to what would be seen for an ideal chain, although it can be seen from figure 1 that the chains are *far from* ideal at this concentration. For higher values of ϕ there is a downturn in the $k^2\hat{\omega}(k)$ curve, consistent with a collapsing of the molecules. The results for $\hat{\omega}(k)$ suggest that the chains are self-avoiding walks at low area fractions and become smaller and almost ideal as the area fraction is increased, before becoming collapsed objects at high area fractions. A careful study of the shape of the chains (see below) suggests, however, that these conclusions are not correct.

The behavior of $\hat{\omega}(k)$ for other chain lengths is qualitatively similar to what is observed for $n = 32$. Figure 4 compares Kratky plots for $n = 16$, 32, and 64 for $\phi = 0.3$. For $n = 16$, the Kratky plot looks similar to what would be observed for an ideal chain. As the chain length is increased, for the same value of ϕ, the chains become more compact. This is expected because the chains are expected to overlap more, at the same area fraction, when the chains are longer. The peak or plateau moves to smaller wave vectors and decreases in magnitude as the chain length is increased, as expected from the analysis of ideal chains.

C. Chain Shape. Although the chains become more compact as the area fraction is increased, they do not, on average, become significantly more disklike. This behavior could not have been anticipated from an analysis of the single chain structure factor. The asphericity of the chains is listed in Tables 1−3. For isolated chains, the asphericity, A_2 is insensitive to the chain length and takes on a value of 0.63−0.64 in all cases. Recall that $A_2 = 1$ for rods and $A_2 = 0$ for disks, so in no case are the chains even close to being disklike.

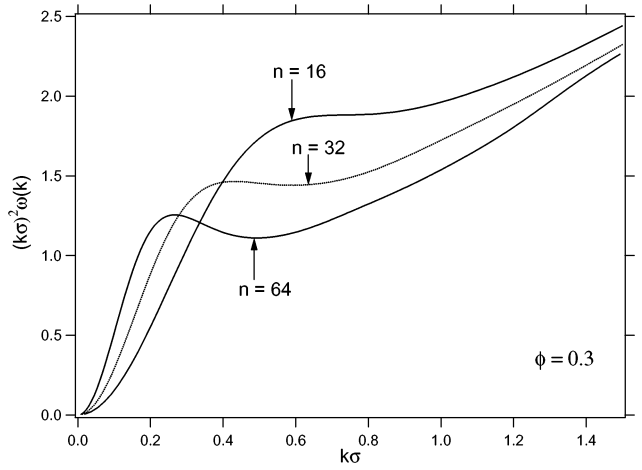

Figure 4. Kratky plot of the single chain structure factor for $\phi = 0.3$ and various chain lengths (as marked).

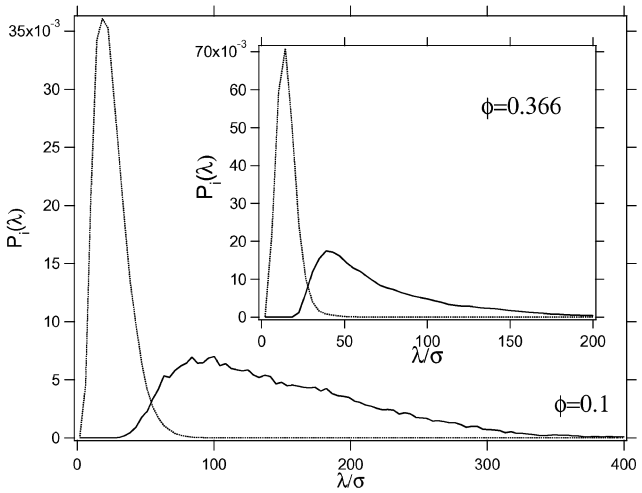

Figure 5. Probability distribution function for the larger (solid line) and smaller (dashed line) eigenvalues of the moment of inertia tensor, for $n = 128$ and $\phi = 0.1$ (main figure) and $\phi = 0.366$ (inset).

For all chain lengths, as the area fraction is increased, A_2 decreases, implying that the chains are becoming more disklike. A_2 changes by only about 10% over the entire range of area fractions, however, implying that the average shape of the chain molecules is *relatively insensitive* to concentration. This behavior is observed for all the chain lengths studied.

Since two-dimensional polymer chains are elliptical in shape, more detailed information regarding the chain shape can be obtained by considering the probability distribution function for the two eigenvalues of the moment of inertia tensor. Figure 5 depicts the probability distribution functions $P_1(\lambda)$ (solid lines) and $P_2(\lambda)$ (dashed lines) for $n = 128$ and for $\phi = 0.1$ and 0.366 (inset). Recall the P_1 (P_2) is the probability distribution function for the larger (smaller) eigenvalue, and the distributions are normalized so that $\int P_i(\lambda)\, d\lambda = 1$. In both cases depicted, $P_2(\lambda)$ is fairly sharply peaked and $P_1(\lambda)$ displays a broader peak and a long tail. This is fairly typical for all the cases investigated. This suggests the chains are elongated and that there are a significant number of chains that are considerably more elongated than the average. It is important that this occurs for both low and high area fractions because it implies that the distribution of shapes is not very different in the dilute and semidilute regimes. This is more clearly seen

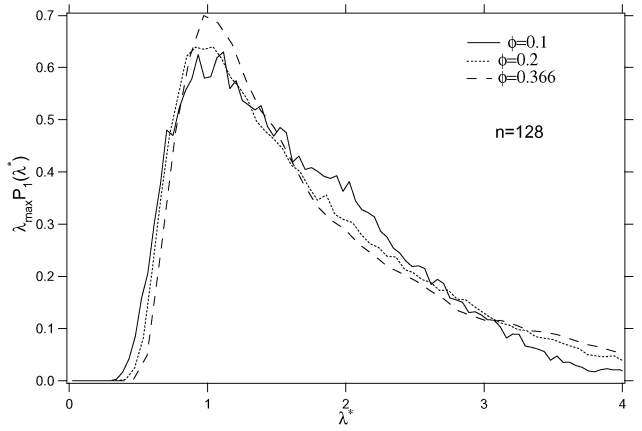

Figure 6. Probability distribution function for the larger eigenvalue (λ_1) of the moment of inertia tensor for $n = 128$ and various area fractions (as marked). λ_{max} is the value of λ_1 at the peak in $P(\lambda_1)$ and $\lambda^* = \lambda_1/\lambda_{max}$.

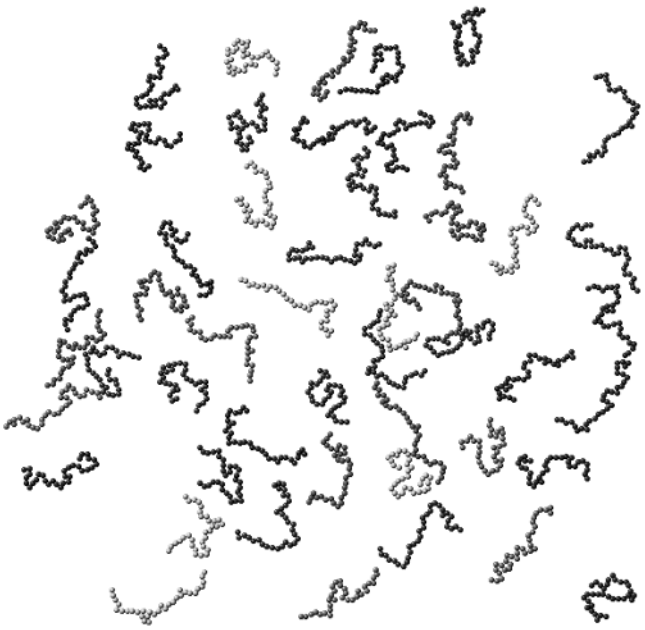

Figure 7. Snapshot of an equilibrated chain configuration for $n = 32$ and $\phi = 0.1$.

in Figure 6, which compares $P_1(\lambda)$ for three area fractions. In the figure, $\lambda^* = \lambda_1/\lambda_{max}$ where λ_{max} is the value of λ_1 at the maximum in $P_1(\lambda)$, and the ordinate is multiplied by λ_{max} in order to preserve the normalization of the distributions. The distribution of the larger eigenvalues is essentially the same at the three area fractions. If anything, as the area fraction is increased, the distribution broadens a little, although this broadening is within statistical uncertainties.

Snapshots of equilibrated configurations for $n = 32$ and $\phi = 0.1$, 0.3, and 0.5 are depicted in Figures 7, 8, and 9, respectively. In the figures, the chain centers of mass have been moved into the primary simulation cell, and only this image is shown, even though in reality the system is replicated in both directions with periodic boundary conditions. The snapshots show that in all cases there a distribution of shapes including some extended and some compact configurations. This is true of even the most dense configuration depicted. Although Figures 7−9 do not contain as much information on chain shape as Figure 6, they help one visualize how a

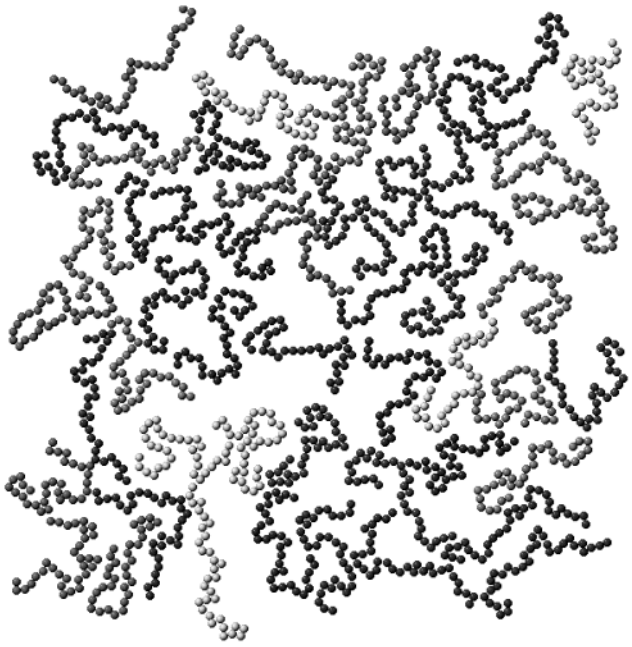

Figure 8. Snapshot of an equilibrated chain configuration for $n = 32$ and $\phi = 0.3$.

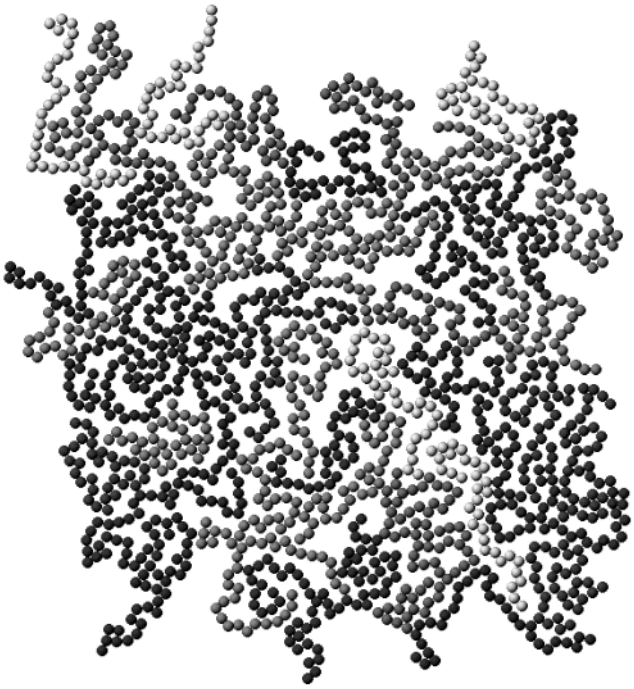

Figure 9. Snapshot of an equilibrated chain configuration for $n = 32$ and $\phi = 0.5$.

distribution of chains shapes makes it easier to pack chains in two-dimensional space.

D. Pair Correlation Functions. For all area fractions and chain lengths, the intermolecular site−site pair correlation function shows a pronounced correlation hole which is a consequence of sites of other chains being excluded from any given site because of the presence of sites from the same chain. As the concentration is increased, however, there is considerable interpenetration between chains. Figure 10 depicts $g(r)$ for $n = 32$ and for $\phi = 0.1$, 0.3, and 0.6. (Note that the abscissa is scaled with the radius of gyration.) In all cases, $g(r) < 1$ as a consequence of the correlation hole effect mentioned above. As the area fraction is increased, the value

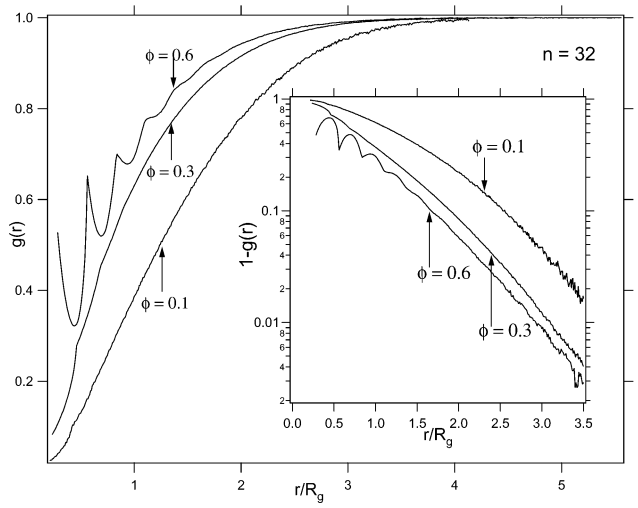

Figure 10. Pair correlation function, $g(r)$, for $n = 32$ and various volume fractions. The inset shows $1 - g(r)$ on a semilog plot.

of $g(r)$ at small separations increases because the chains begin to pack among each other more efficiently. Since R_g also decreases as the area fraction is increased, the increased importance of packing effects as the area fraction is increased is more marked than appears in the figure, where the abscissa is normalized with R_g. At high densities there is strong intermolecular packing of the chains, and this is manifested in strong and sharp peaks in $g(r)$ at high densities ($\phi \geq 0.5$). For example, for $\phi = 0.6$ six solvation shells are clearly seen. The fact that $g(\sigma^+)$ takes on significantly nonzero values (for example, $g(\sigma^+) = 0.86$ for $n = 32$ and $\phi = 0.65$) implies that there is significant interpenetration of chains. There are also some distinct differences from three-dimensional chains. For example, $g(r)$ is always less than 1, whereas in three-dimensional hard chains, at high densities, $g(r)$ takes on values much greater than 1. The solvation shells are also more pronounced in two-dimensional systems when compared to three-dimensional systems at similar volume/area fractions.

At large distances, the behavior of $g(r)$ is consistent with the form

$$g(r) = 1 - c \exp\left(-\alpha \frac{r}{R_g}\right) \tag{12}$$

suggested by Cavallo et al.,[15] where c and α are constants. To a good approximation, α is independent of chain length and area fraction, and c is independent of chain length but dependent on area fraction. Figure 11 depicts $1 - g(r)$ vs r/R_g on a semilog plot for $\phi = 0.5$ and for $n = 16$, 32, and 64. For large r/R_g all the curves collapse, suggesting universal behavior in the pair correlation function with a correlation hole that is of the order of the size of the chain.

E. Equation of State. The reduced pressure, $p^* \equiv \beta p \sigma^3$, depends on chain length at low area fractions but becomes independent of n for large area fractions. According to scaling theory, a plot of p^*/p^{id} vs ϕ/ϕ^*, where p^{id} is the (dimensionless) pressure of an ideal gas of chains at a volume fraction ϕ ($p^{id} \equiv \rho\sigma^3$), should be a universal curve for all chain lengths. However, such as plot does *not* collapse the data, suggesting that the scaling prediction is not valid for the chain lengths studied. This is consistent with the observations of

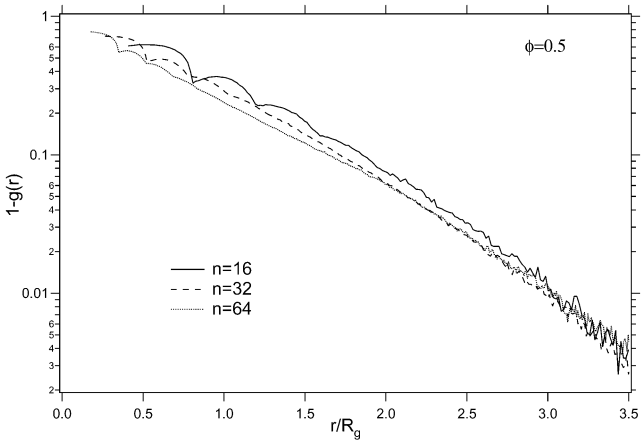

Figure 11. Semilog plot of $1 - g(r)$ for $\phi = 0.5$ and various n.

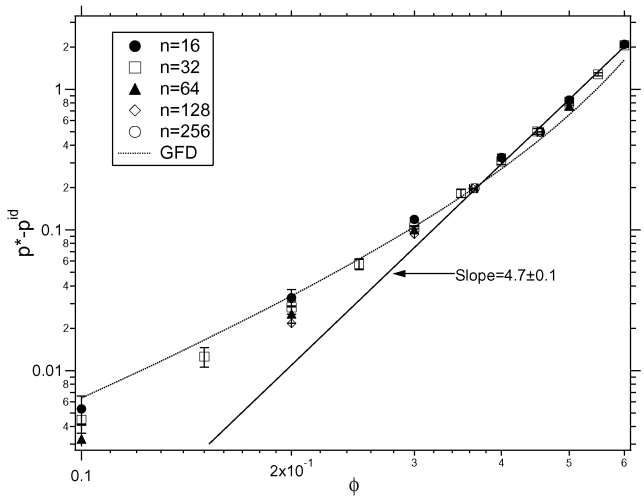

Figure 12. Equation of state of two-dimensional polymer melts. Variation of reduced pressure with area fraction for various n. The solid line is a fit to the data for $n \geq 64$ and $p^* > 0.2$ with slope as marked. The dotted line is the prediction of the generalized Flory dimer (GFD) equation of state[18] for $n = 256$.

Dickman[8] in his lattice simulations for $n \leq 180$. To isolate packing effects on the pressure, we plot $p^* - p^{id}$ as a function of ϕ in Figure 12. For low area fractions, $p^* - p^{id}$ displays a slight chain length dependence and does not show power law behavior with ϕ. For high area fractions, the pressure becomes insensitive to the chain length, similar to what was seen in simulations of lattice chains.[8] The solid line in Figure 12 is a least-squares fit to the data for $p^* - p^{id} \geq 0.2$. A good fit is obtained, and the data are consistent with $p \sim f^{4.7\pm0.1}$. This variation of pressure with concentration is considerably stronger than the scaling $p \sim c^{2.25}$ seen for three-dimensional polymer melts and the scaling theory prediction of $p \sim \phi^3$. The dotted line in Figure 12 is the prediction of the generalized Flory dimer (GFD) equation of state.[18] In this equation of state the pressure is a very weak function of n for the chain lengths considered, and the prediction for $n = 256$ is depicted. The GFD equation of state is in quantitative agreement with the simulations over the entire range of area fractions, although it overestimates the pressure at low area fractions.

IV. Summary and Conclusions

Off-lattice Monte Carlo simulation results are presented for the static properties of two-dimensional polymer solutions and melts. The conformational, structural, and volumetric properties are reported for a range of area fractions and chain lengths. To our knowledge, this is the first study of this nature for two-dimensional polymers. The simulations reveal some interesting features of two-dimensional polymer solutions. For example, the chain size increases with increasing concentration at very high area fractions. This behavior is predicted by self-consistent integral equation theory for three-dimensional polymers but has never before been observed. We also find that an analysis of the structure factor in standard Kratky fashion, which suggests that chains are ideal at intermediate concentrations and collapsed at higher concentrations, is misleading. A more detailed analysis of chain shape shows instead that the shape of the chains does not change significantly as the concentration is increased. In fact, the asphericity changes by less than 10% over the entire range of concentrations, and the distribution of chain shapes is broad at all concentrations.

The simulations do not support two popular models of chain behavior in two-dimensional systems. There have been two approaches to understanding the properties of two-dimensional polymer solutions and melts. In the scaling approach, it is assumed that the chains interpenetrate in semidilute solutions and that the correlation length is independent of the degree of polymerization.[6] In the second approach[5] it is argued that the chains form segregated collapsed disks. Both these models predict the same scaling behavior for the chain size, which is also observed in the simulations. The simulations do not support the picture of two-dimensional chains as segregated fluctuating disklike objects at high concentrations. Instead, there is considerable interpenetration of chains manifested in a fairly high value of $g(r)$ at contact ($g(\sigma^+) \approx 0.85$ for $n = 32$ and $\phi = 0.6$). The simulations do not support the scaling picture either, and the pressure displays a much stronger concentration dependence ($p \sim c^{4.7\pm0.1}$) than predicted by scaling theory ($p \sim c^3$). Of course, the scaling theory is expected to be valid only in the regime $\phi^* \ll \phi \ll 1$. For two-dimensional systems these conditions, which are satisfied only for very long chains, might be difficult to attain in simulations or experiment.

In conclusion, we find that the conformational and structural properties of two-dimensional polymer solutions are more complex than previously thought and that some ideas regarding these systems might require reconsideration. As a caveat, we have studied a very simple model of polymers, and it is conceivable that the properties are sensitive to the details of molecular architecture and interactions. We have not studied the dynamic properties either, although the observed distribution of chain shapes suggests that the dynamics could be very interesting. We hope that this work will motivate future research on a rich and interesting area of polymer science.

Acknowledgment. I thank Dr. Marcus Müller for helpful discussions, a critical reading of the manuscript, and for providing a copy of ref 15 prior to publication. This material is based upon work supported by the National Science Foundation under Grant CHE-0315219.

References and Notes

(1) Yethiraj, A. *Adv. Chem. Phys.* **2002**, *121*, 89 and references therein.

(2) Maier, B.; Radler, J. O. *Phys. Rev. Lett.* **1999**, *82*, 1911.
(3) Maier, B.; Radler, J. O. *Macromolecules* **2000**, *33*, 7185.
(4) Maier, B.; Radler, J. O. *Macromolecules* **2001**, *34*, 5723.
(5) De Gennes, P.-G. *Scaling Concepts in Polymer Physics*; Cornell University Press: Ithaca, NY, 1979.
(6) Des Cloizeaux, J.; Jannink, G. *Polymers in Solution*; Oxford Science Publications: Oxford, 1990.
(7) Nikamarov, E. S.; Obukhov, S. P. *Sov. Phys. JETP* **1981**, *53*, 328.
(8) Dickman, R. *J. Chem. Phys.* **1989**, *91*, 454.
(9) Dickman, R. *J. Chem. Phys.* **1992**, *96*, 1516.
(10) Carmesin, I.; Kremer, K. *J. Phys. (Paris)* **1990**, *51*, 915.
(11) Reiter, J.; Zifferer, G.; Olaj, O. F. *Macromolecules* **1989**, *22*, 3120.
(12) Nelson, P. H.; Hatton, T. A.; Rutledge, G. C. *J. Chem. Phys.* **1997**, *107*, 1269.
(13) Teraoka, I.; Wang, Y. *Macromolecules* **2000**, *33*, 6901.
(14) Ostrovsky, B.; Smith, M. A.; Bar-Yam, Y. *Int. J. Mod. Phys. C* **1997**, *8*, 931.
(15) Cavallo, A.; Müller, M.; Binder, K. *Europhys. Lett.* **2003**, *61*, 214.
(16) Dickman, R.; Hall, C. K. *J. Chem. Phys.* **1986**, *85*, 4108.
(17) Reiter, J.; Duering, E. R. *Macromol. Theory Simul.* **1995**, *4*, 667.
(18) Honnell, K. G.; Hall, C. K. *J. Chem. Phys.* **1989**, *90*, 1841.
(19) Kushwaha, K. B.; Khanna, K. N. *Mol. Phys.* **1999**, *97*, 907.
(20) Yethiraj, A.; Hall, C. K. *Macromolecules* **1990**, *23*, 1865.
(21) Yethiraj, A. *J. Chem. Phys.* **1994**, *101*, 9104.
(22) Dickman, R.; Hall, C. K. *J. Chem. Phys.* **1988**, *89*, 3168.
(23) De Pablo, J. J.; Laso, M.; Suter, U. W. *J. Chem. Phys.* **1992**, *96*, 2395.
(24) Wall, F. T.; Mandel, F. *J. Chem. Phys.* **1975**, *63*, 4592.
(25) Frenkel, D.; Smit, B. *Understanding Molecular Simulation: From Algorithms to Applications*; Academic Press: San Diego, 2002.
(26) Gaspari, G.; Rudnick, J.; Beldjenna, A. *J. Phys. A: Math. Gen.* **1987**, *20*, 3393.
(27) McQuarrie, D. A. *Statistical Mechanics;* Harper and Row: New York, 1976.
(28) Chang, J.; Sandler, S. I. *Chem. Eng. Sci.* **1994**, *49*, 2777.
(29) Grayce, C. J.; Yethiraj, A.; Schweizer, K. S. *J. Chem. Phys.* **1994**, *100*, 6857.
(30) Doi, M.; Edwards, S. F. *The Theory of Polymer Dynamics*; Oxford Science Publications: Oxford, 1986.

MA025907R